Mid-wavelength InAs/GaSb type-II superlattice barrier detector with nBn design and M barrier*

LIU Zhaojun[1], ZHU Lianqing[2], LU Lidan[2], DONG Mingli[2], ZHANG Dongliang[3]**, and ZHENG Xiantong[3]**

1. *School of Opto-Electronic Engineering, Changchun University of Science & Technology, Changchun 130022, China*
2. *Key Laboratory of the Ministry of Education for Optoelectronic Measurement Technology and Instrument, Beijing Information Science & Technology University, Beijing 100192, China*
3. *Key Laboratory of Optical Fiber Sensing and System, Beijing Information Science & Technology University, Beijing 100016, China*

(Received 25 February 2023; Revised 22 March 2023)
©Tianjin University of Technology 2023

This study reports the performance of an InAs/GaSb type-II superlattices (T2SLs) detector with nBn structure for mid-wavelength infrared (MWIR) detection. An electronic band structure of M barrier is calculated using 8-band k·p method, and the nBn structure is designed with the M barrier. The detector is prepared by wet etching, which is simple in manufacturing process. X-ray diffraction (XRD) and atomic force microscope (AFM) characteristics indicate that the detector material has good crystal quality and surface morphology. The saturation bias of the spectral response measurements at 77 K is 300 mV, and the device is promising to work at a temperature of 140 K. Energy gap of T2SLs versus temperature is fitted by the Varshni curve, and zero temperature bandgap $E_g(0)$, empirical coefficients α and β are extracted. A dark current density of 3.2×10^{-5} A/cm^2 and differential resistance area (RA) product of 1.0×10^4 Ω·cm^2 are measured at 77 K. The dominant mechanism of dark current at different temperature ranges is analyzed. The device with a 50% cutoff wavelength of 4.68 μm exhibits a responsivity of 0.6 A/W, a topside illuminated quantum efficiency of 20% without antireflection coating (ARC), and a detectivity of 9.17×10^{11} cm·Hz$^{1/2}$/W at 77 K and 0.3 V.

Document code: A **Article ID:** 1673-1905(2023)10-0577-6
DOI https://doi.org/10.1007/s11801-023-3032-y

In recent years, there has been significant progress in the development of mid-wavelength infrared (MWIR) detectors. They are used in a variety of applications, including spectroscopy, thermal imaging, and environmental monitoring. Type−II superlattices (T2SLs) based on the narrow-bandgap semiconductors of the InAs/GaSb/AlSb system have emerged as one of the top candidates for third-generation infrared (IR) detection technology[1-4]. New detector architectures require multispectral detection, high detectivity, small size, low weight, low power consumption (SWaP), and operation at a high temperature, significantly reducing the size and total cost of the detector system. The antimonide-based T2SLs have the potential advantages for the realization of high-performance large area focal plane arrays due to the flexibility of bandgap engineering, high material uniformity, and reduced tunneling currents[5,6]. Type-II "misaligned" band alignment of InAs and GaSb means the spatial separation of electrons and holes, which decreases the Auger recombination rate and enhances the high operating temperature (HOT) device operation[7-11].

Various combination based on the 6.1 Å family (InAs/GaSb/AlSb) provides considerable flexibility in forming a variety of alloys and superlattices. There are several barrier infrared detector structures, including nBn, W-structure, complementary barrier infrared detector (CBIRD) and PBINN, among which nBn is one of the typical representatives[12-14]. The valence band offset (VBO) between the absorption region and the barrier of nBn structure is nearly zero, which allows the minority carriers to pass through well, while the large conduction band offset blocks the flow of majority carriers[15-17]. The nBn structure device has the advantage of low dark current and high temperature operation, and it is significant to design the barrier structure that matches with the InAs/GaSb T2SLs.

The commonly used barrier structure in nBn structure is AlGaSb barrier. The zero VBO can be adjusted by

* This work has been supported by the Beijing Scholars Program (No.74A2111113), the National Natural Science Foundation of China (No. 62205029), the Young Elite Scientist Sponsorship Program by the China Association for Science and Technology (No.YESS20200146), and the Beijing Natural Science Foundation (No.4202027).
** E-mails: lqzhu_bistu@sina.com; zdl_photonics@bistu.edu.cn

adjusting the mole fraction which is a little difficult. Besides, the lattice mismatch between AlGaSb and InAs/GaSb T2SLs may cause defects related to strain, which adversely affects the performance. MARTYNIUK et al[18] reported the MWIR InAs/GaSb T2SLs nBn-$Al_{0.2}Ga_{0.8}Sb$ barrier detector's photoelectrical performance, the differential resistance area (*RA*) product and detectivity reached values of 1 000 Ω·cm^2 and 4×10^{11} cm·Hz$^{1/2}$/W at 77 K. The energy band structure can be adjusted by inserting large bandgap AlSb into the GaSb layer of InAs/GaSb T2SLs, and the shape of the energy band structure is similar to letter "M", which is called M structure[19]. The hole quantum well can be separated into two parts, and it can be tailored to achieve the required infrared bandgap based on theoretical calculation. AlSb with a larger bandgap suppresses the interaction between adjacent InAs quantum wells, reducing the tunneling effect of electrons. On the other hand, a unipolar barrier with M structure can inhibit the flow of the majority carrier but allow the unimpeded flow of the additional[20-22]. Diffusion and dark current associated with Shockley-Read-Hall in the depletion region can be suppressed[23,24]. The M barrier composed of InAs/GaSb/AlSb is considered to be a promising barrier structure[24,25]. Binh-Minh Nguyen presents a PπMN T2SLs detector with the M structure barrier, which can significantly reduce the dark current.

In terms of device processing, there are various passivation methods to overcome surface leakage currents, such as the deposition of silicon dioxide layer and overgrowth with wide bandgap material[26-29]. Atomic layer deposited (ALD) aluminum oxide (Al_2O_3) has emerged as a novel passivation approach of T2SLs' MWIR single-pixel photodetector. Its advantages include perfect conformal coverage even at sharp edges, considerable area thickness uniformity, very low process temperatures, and plasma-free operation[30]. On the other hand, the device wet processing technology is nimble in process, short in cycle, and can realize the preparation of high-performance devices without relying on complex equipment.

In this paper, we report an MWIR InAs/GaSb T2SLs nBn detector with M barrier and ALD deposited Al_2O_3 passivation. Firstly, we systematically introduce the device design and process, and analyze the crystal quality and morphology of the device material. An electronic band structure of M structure is calculated using 8-band k·p method, and the nBn structure is designed with the M barrier. The epitaxial growth and processing process of M barrier structure are close to those of InAs/GaSb, and the device is processed by wet process technology. Secondly, spectral response measurements are performed at different applied biases and temperatures. Temperature-dependent dark current, responsivity, quantum efficiency, and detectivity of the nBn MWIR detector are investigated, and the Arrhenius plot analyzes the dark current mechanisms.

The device structure is grown on n-type doped GaSb (100) substrates by ultrahigh vacuum molecular beam epitaxy (MBE) system (Komponenten Octoplus 400), as shown in Fig.1(a). It consists of a 500-nm-thick n-type GaSb buffer (GaTe, n~10^{18} cm^{-3}), followed by a 450-nm-thick n-type T2SLs bottom contact layer (Si, n~10^{18} cm^{-3}), a 2-μm-thick T2SLs absorber layer, 105-nm-thick M barrier structure, a 200-nm-thick n-type T2SLs top contact layer (Si, n~10^{18} cm^{-3}), and a 20-nm-thick n-type InAs cap layer (Si, 10^{18} cm^{-3}). The GaSb substrate is deoxidized at 520 °C for 10 min to remove the naturally generated oxide film, and Sb-rich atmosphere protection is required when the temperature exceeds 300 °C. The growth temperature of GaSb buffer layer is 440 °C, and the growth temperature of absorption region and barrier region is 420 °C. The V/III beam flux ratios of the InAs and GaSb growth are 10 and 5, respectively. Eight monolayers (MLs) InAs and six MLs GaSb with a 50% cutoff wavelength of 5 μm at room temperature is designed. The epitaxial growth condition of the M structure is similar to the T2SLs, and heterostructure can be experimentally realized without growth difficulty. The M structure composed of 3 MLs InAs/2 MLs GaSb/3 MLs AlSb/2 MLs GaSb with a wider bandgap of ~0.9 eV can provide 0.02 eV VBO and a large conduction band offset of 0.57 eV, as shown in Fig.1(b). The large conduction band offset blocks the majority carrier current, while photogenerated minority carriers can pass through and generate photocurrent[31].

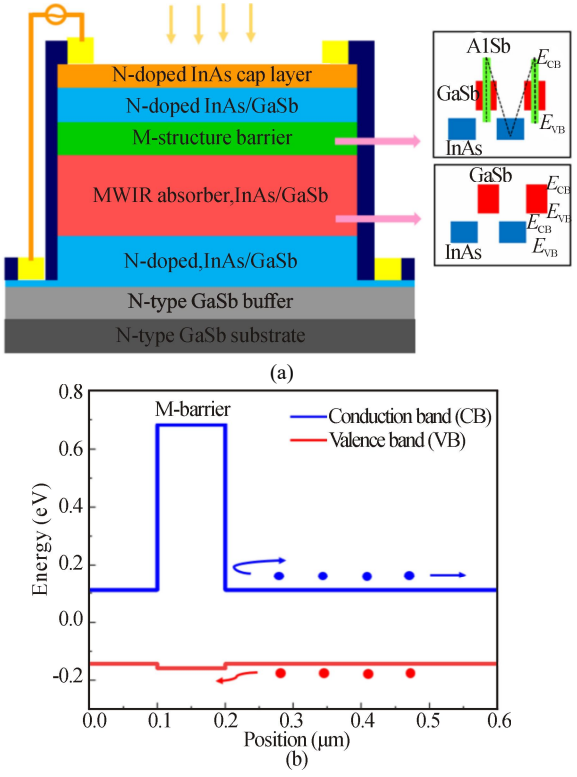

Fig.1 (a) Structure diagram of InAs/GaSb T2SLs MWIR nBn detector with M barrier; (b) Bandgap diagram of nBn detector

The nBn structure is processed into single-element devices by standard optical lithography and wet chemical etching. The corrosion solution is $C_6H_8O_7 \cdot H_2O$: H_3PO_4: H_2O_2: H_2O, with the ratio of 7.3 g: 2 mL: 4 mL: 80 mL. Mesa-sidewalls are passivated with a dielectric layer of Al_2O_3 film deposited by ALD to suppress the surface leakage current. Next the Al_2O_3 film is removed with 85% H_3PO_4 at 80 °C to expose the surface, excluding the mesa sidewall. Ti (10 nm, wetting layer)/Au (100 nm) deposited by e-beam evaporation and a standard lift-off process are used to realize ohmic contact.

The high-resolution X-ray diffraction (XRD) curve of the ω-2θ scan at the GaSb (004) reflection of the nBn detector is displayed in Fig.2. The scanning angle is 8°, and the step length is 0.001° with 0.5 s residence time. The 0th satellite peaks of the T2SL and M barrier structures are located on both sides of the substrate peak, subjected to tensile strain and compression strain, respectively. The tertiary satellite peak of T2SL structure and the secondary satellite peak of M barrier structure are visible clearly. The slight separation of the satellite peaks corresponds to the T2SL structures located at the upper and lower of the M barrier. The period thicknesses of the two T2SL structures are the same of 4.44 nm, while the strain is different. The full width at half maximum (*FWHM*) of the substrate peak, 0th satellite peaks of T2SL structure and M barrier structure measured in Ω mode are 23.9, 32.9, and 155.8 arcseconds, respectively.

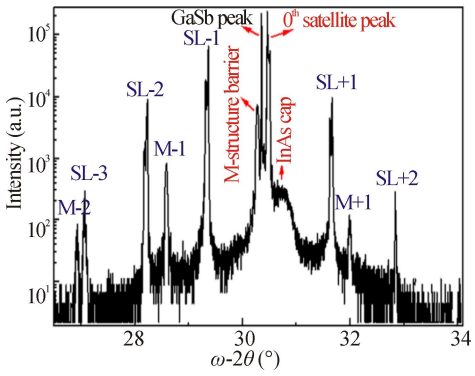

Fig.2 XRD pattern of the *ω-2θ* scan around the GaSb (004) reflection

Good crystal quality and surface appearance are the first steps in preparation for large focal plane arrays. Fig.3(a) and (b) show the atomic force microscope (AFM) morphology of 50 μm×50 μm and 5 μm×5 μm scan area with a minor root mean squares (*RMS*) roughness and clear atomic step. The amplitude of the AFM probe is 21.8 nm, and the Q-factor is 425.

Spectral response measurements are performed on the different applied biases at 77 K, as shown in Fig.4. The water vapor absorption in the system may cause a significant depression in the response spectrum. The right depression is the absorption peak of CO_2. When the applied bias is under 150 mV, due to the existence of a small VBO, the photogenerated carriers cannot pass through, and the spectral response intensity is near zero. The increase of the applied bias will lead to tunneling and energy band tilt, so the carriers will cross the valence band and the spectral response will be enhanced. The spectral response intensity increases and is close to saturation at 300 mV, indicating the device's best working point.

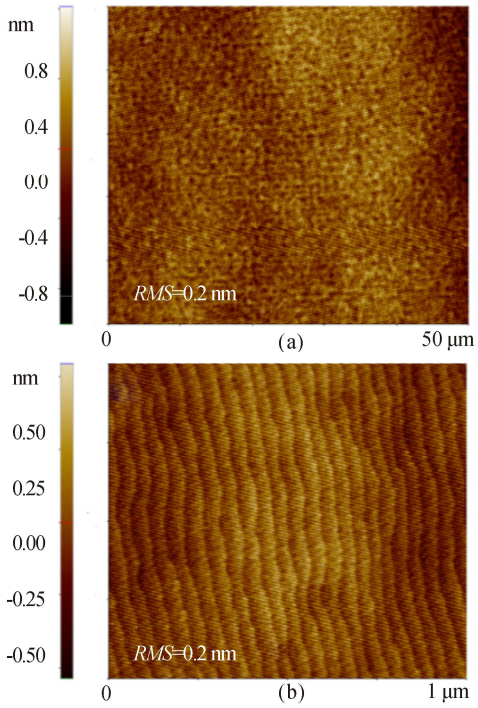

Fig.3 (a) AFM morphology of 50 μm×50 μm scan area; (b) AFM morphology of 1 μm×1 μm scan area

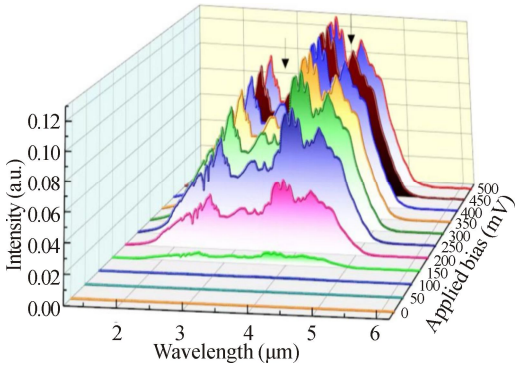

Fig.4 Optical spectra with different applied biases at 77 K

Fig.5 shows the spectral response of nBn detector at different temperatures. The bias is 0.3 V and the diameter of the detector mesa is 200 μm. The response spectrum intensities at 70 K to 140 K are close to saturation, indicating that the device is promising to work at a high-temperature environment of 140 K. The intensity of the response spectrum declines when the temperature is higher than 160 K, and there is still a weak response intensity when the temperature is close to

room temperature.

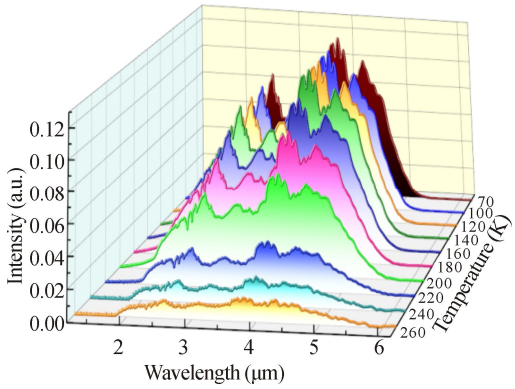

Fig.5 Spectral responses of nBn detector at different temperatures with applied bias of 0.3 V

Normalize the response spectrum of Fig.5, and the 50% cutoff wavelength at 77 K and 280 K are 4.68 μm and 4.97 μm, respectively. The T2SL's bandgap energy, extracted from the normalized spectral response, as a function of temperature is shown in Fig.6. As the temperature rises, the bandgap decreases, and the wavelength red shifts correspondingly. The fitting curve is plotted using the well-known Varshni equation as follows

$$E_g(T) = E_g(0) - \frac{\alpha T^2}{\beta + T}. \quad (1)$$

$E_g(0)$=0.26 eV is the gap energy at zero temperature. Debye temperature β=260 K and α=1.434 5e^{-4} eVK^{-1} are the intrinsic constants of materials.

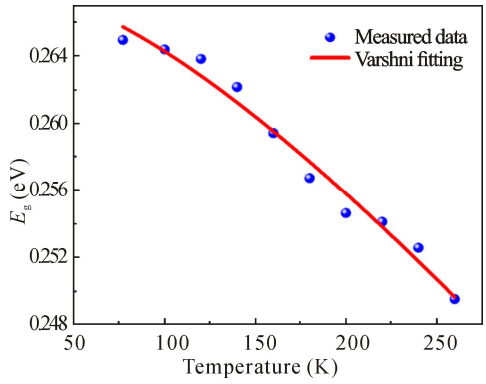

Fig.6 Energy gap of T2SLs versus temperature and the Varshni fitting curve

Electrical dark current significantly limits the performance of infrared detectors. Fig.7 shows the dark current density (J_d) and *RA* as a function of applied bias for temperatures ranging from 77 K to 280 K. The dark current density is 3.2×10^{-5} A/cm^2 and *RA* is 1.0×10^4 Ω·cm^2 at 77 K and 0.3 V positive bias. The dark current of the device increases, and the *RA* decreases as the temperature rises. *RA* value of the device reaches the maximum near the zero bias. The rapid reduction of *RA* between 0 to 0.2 V is caused by the tunnel of the carrier, indicating that the device is under the tunnel dark current mechanism. *RA* increases and becomes stable when the voltage gradually increases to 0.3 V. The device's VBO is close to zero, and the cave carrier can be easily circulated. The working point of the device is achieved at 0.3 V, which is consistent with spectral response measurement.

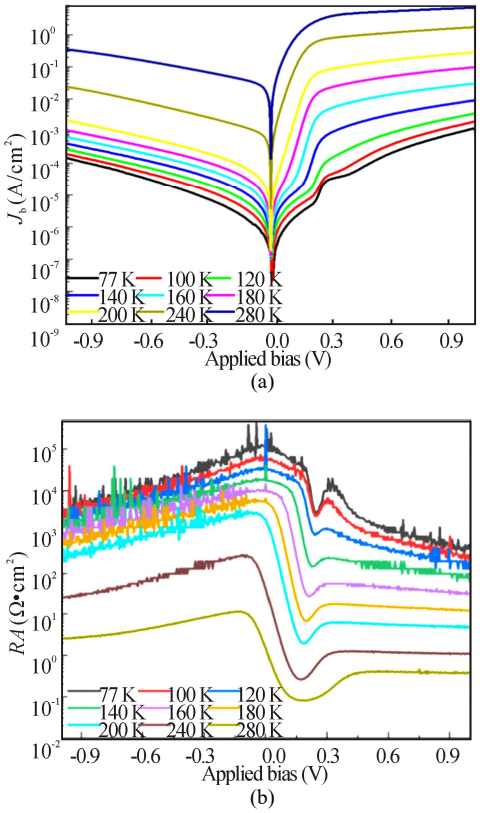

Fig.7 (a) Dark current density and (b) dynamic *RA* versus applied bias at different temperatures

The identification of dark current mechanisms, such as diffusion, generation-recombination (GR), band-to-band tunneling (BTB), trap-assisted tunneling (TAT), and surface leakage currents, is essential for the understanding of electrical properties and improving T2SL's device performances. The Arrhenius plot of J_d versus the inverse temperature (1 000/T) according to Eq.(2) has been shown in Fig.8.

$$J_{DARK}(T) \propto \exp\left(\frac{-E_a}{K_B T}\right), \quad (2)$$

where K_B is the Boltzmann constant and E_a is the activation energy. The fitted activation energy (E_a) is 225 meV for T>180 K, which roughly agrees with the energy bandgap of the absorber region of 248 meV, as determined from the 50% cutoff wavelength of 5 μm. As shown in Eq.(2), diffusion current has the most significant temperature dependence. The dark current in the device is diffusion current and a part of GR current above 180 K. E_a is fitted to be 142 meV from 120 K to 160 K, roughly half of the designed absorber energy bandgap. This indicates that the GR dark current becomes dominant, and there is

also a certain amount of tunneling current. At low temperatures, E_a is only 25 meV, which reveals the dark current is primarily due to the temperature-insensitive tunneling current or surface leakage current.

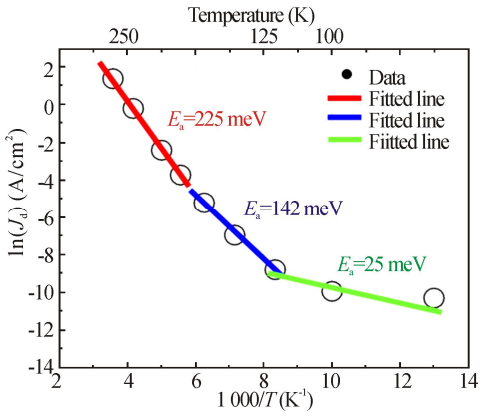

Fig.8 Arrhenius plot of J_d versus the inverse temperature (1 000/*T*) at 0.3 V

Fig.9 presents the responsivity and quantum efficiency characteristics of nBn device at 77 K. The device has not been started up, and the responsivity is close to zero when the applied bias is less than 200 mV, consistent with the spectral response curve of Fig.3. The responsivity gradually increases and stabilizes at about 0.6 A/W. The quantum efficiency is 22% without an antireflection coating (ARC) measured at 4 μm. The detectivity is calculated by

$$D^* = R / \sqrt{4KT / R_d A}, \quad (3)$$

where R is the responsivity, R_dA is the product of dynamic resistance and area at 0.3 V, and K is Boltzmann's constant. The detectivity decreases with the temperature increase, and is about 9.17×10^{11} cm·Hz$^{1/2}$/W at 77 K and 0.3 V. Detectivity is a comprehensive evaluation of quantum efficiency and dark current, and the adjustment of the two has the opposite trend[32]. It is still necessary to improve quantum efficiency of the device by designing the thickness of absorption region and the energy band engineering, and reduce the dark current by improving the material quality which is related with the defect state and optimizing the device processing technology.

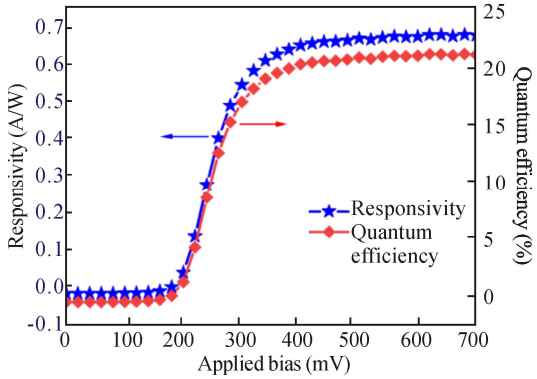

Fig.9 Responsivity and quantum efficiency as a function of applied bias at 77 K

In summary, we systematically introduce the device preparation and characterization of the M barrier nBn detector obtained by a wet process. The T2SLs structure is designed of 8 MLs InAs and 6 MLs GaSb, and the M barrier structure is composed of 3 MLs InAs/2 MLs GaSb/3 MLs AlSb/2 MLs GaSb with a bandgap of ~0.9 eV. The intensities of spectral response below 140 K have no significant change, indicating that the device can be used in high operating temperatures. $E_g(0)$=0.26 eV, β=260 K, and α=1.434 5e^{-4} eVK^{-1} are extracted from the Varshni fitting curve. The dark current density is 3.2×10^{-5} A/cm^2 and the differential resistance area product is 1.0×10^4 Ω·cm^2 at 0.3 V and 77 K. The detector's dominant dark current mechanism is different and varies with different temperature regimes. The responsivity is about 0.6 A/W, and the quantum efficiency of 2-μm-thick absorption region is 22% without an ARC measured at 4 μm. The detectivity is about 9.17×10^{11} cm·Hz$^{1/2}$/W at 77 K and 0.3 V. Although a small VBO exists in the energy band of the device, the detectivity is still considerable. It still has great potential to enhance the detector performance by optimizing the energy band and processing technology. In conclusion, InAs/GaSb T2SLs nBn detectors with M barrier are promising candidates for infrared focal plane array detectors.

Ethics declarations

Conflicts of interest

The authors declare no conflict of interest.

References

[1] ROGALSKI A, MARTYNIUK P. Mid-wavelength infrared nBn for HOT detectors[J]. Journal of electronic materials, 2014, 43(8): 2963-2969.

[2] LIU Z, ZHAO Z F, GUO H M, et al. Band structure and optical absorption in InAs/GaSb quantum well[J]. Acta physica sinica, 2012, 61(21): 217303.

[3] MANYK T, HACKIEWICZ K, RUTKOWSKI J, et al. Theoretical simulation of T2SLs InAs/GaSb cascade photodetector for HOT condition[J]. Journal of semiconductors, 2018, 39(9): 38-41.

[4] LIU Z J, ZHU L Q, ZHENG X T, et al. Interface effect on superlattice quality and optical properties of InAs/GaSb type-II superlattices grown by molecular beam epitaxy[J]. Chinese physics B, 2022, 31(12): 128503.

[5] MANASREH M O. Antimonide-related strained-layer heterostructures[J]. Lasers optics & photonics, 1997.

[6] HUANG J L, YAN S L, XUE T, et al. Mid-wavelength InAs/InAsSb superlattice photodetector with background limited performance temperature higher than 160 K[J]. IEEE transactions on electron devices, 2022, 69(8).

[7] LI H, ZHANG Q, QI X, et al. High resolution X-ray diffraction study in InAs/GaSb superlattice[J]. Ferroelectrics, 2022, 596(1): 86-94.

[8] SUN Y R, DONG J R, HE Y, et al. A six-junction GaAs laser power converter with different sizes of active aperture[J]. Optoelectronics letter, 2017, 13(1)：21-24.

[9] YU H L, WU H Y, ZHU H J, et al. Molecular beam epitaxy of zero lattice-mismatch InAs/GaSb type-II superlattice[J]. Chinese physics letter, 2016, 33(12)：142-145.

[10] WANG Y B, XU Y, ZHANG Y, et al. Effect of compensation doping on the electrical and optical properties of mid-infrared type-II InAs/GaSb superlattice photodetectors[J]. Chinese physics B, 2011, 20(6)：6.

[11] ZHU H, LIU J, ZHU H, et al. High operating temperature InAs/GaSb superlattice based mid wavelength infrared photodetectors grown by MOCVD[J]. Photonics, 2021, 8(12).

[12] VURGAFTMAN I, AIFER E H, CANEDY C L, et al. Graded band gap for dark-current suppression in long-wave infrared W-structured type-II superlattice photodiodes[J]. Applied physics letter, 2006, 89(12)：4757.

[13] HILL C J, SOIBEL A, KEO S A, et al. Growth and performance of superlattice-based long wavelength complementary barrier infrared detectors (CBIRDs)[J]. SPIE proceedings, 2010, 7660.

[14] AIFER E H, WARNER J H, STINE R R, et al. Passivation of W-structured type-II superlattice long-wave infrared photodiodes[J]. SPIE proceedings, 2007, 6542.

[15] MENG C, LI J, YU L, et al. Investigation of a noise source and its impact on the photocurrent performance of long-wave-infrared InAs/GaSb type-II superlattice detectors[J]. Optics express, 2020, 28(10)：14753-14761.

[16] LEE H J, KO S Y, KIM Y H, et al. Strain-induced the dark current characteristics in InAs/GaSb type-II superlattice for mid-wave detector[J]. Journal of semiconductors, 2020, 41(6)：062302.

[17] CUI S N, CHEN W Q, JIANG D W, et al. Dark current simulation and analysis for InAs/GaSb long wavelength infrared barrier detectors[J]. 2022, 121：104006.

[18] MARTYNIUK P, WROBEL J, PLIS E, et al. Performance modeling of MWIR InAs/GaSb/B-$Al_{0.2}Ga_{0.8}Sb$ type-II superlattice nBn detector[J]. Semiconductor science & technology, 2012, 27(5)：55002-55011.

[19] NGUYEN B M, RAZEGHI M, NATHAN V, et al. Type-II M structure photodiodes：an alternative material design for mid-wave to long wavelength infrared regimes[J]. Quantum sensing and nanophotonic devices IV, 2007, 6479：10.

[20] LI N, CHEN W, ZHENG D, et al. The investigations to eliminate the bias dependency of quantum efficiency of InGaAsSb nBn photodetectors for extended short wavelength infrared detection[J]. Infrared physics & technology, 2020, 111：103461.

[21] NGUYEN B M, HOFFMAN D, HUANG K W, et al. Background limited long wavelength infrared type-II InAs/GaSb superlattice photodiodes operating at 110 K[J]. Applied physics letter, 2008, 93(12)：085316.

[22] WANG F, CHEN J, XU Z. et al. Performance comparison between the InAs-based and GaSb-based type-II superlattice photodiodes for long wavelength infrared detection[J]. Optics express, 2017, 25(3)：1629-1635.

[23] GAUTAM N, MYERS S, BARVE A V, et al. Band engineered HOT midwave infrared detectors based on type-II InAs/GaSb strained layer superlattices[J]. Infrared physics & technology, 2013, 59：72-77.

[24] JANG A, LEE H J, KIM Y C, et al. Electrical characteristics of a Ga-free T2SL mid-wave infrared nBn detector based on an InAs/AlAsSb/InAsSb barrier[J]. Journal of electronic materials, 2022, 9：51.

[25] CERVERA C, JAWOROWICZ K, AT-KACI H, et al. Temperature dependence performances of InAs/GaSb superlattice photodiode[J]. Infrared physics & technology, 2011, 54(3)：258-262.

[26] HOANG A H, DEHZANGI A, ADHIKARY S, et al. High performance bias-selectable three-color short-wave/mid-wave/ long-wave infrared photodetectors based on type-II InAs/GaSb/AlSb superlattices[J]. Scientific reports, 2016, 6：24144.

[27] PLIS E, RODRIGUEZ J B, LEE S J, et al. Electrochemical sulphur passivation of InAs/GaSb strain layer superlattice detectors[J]. Electronics letter, 2006, 42(21).

[28] KIM H S. Dark current analysis of an InAs/GaSb type II superlattice infrared photodiode with SiO_2 passivation[J]. Journal of the Korean Physical Society, 2021, 78(11)：1141-1146.

[29] KIM H S. Performance of an InAs_GaSb type-II superlattice photodiode with Si_3N_4 surface passivation[J]. Current optics and photonics, 2021, 5(2)：129-133.

[30] SUZUKI R, OZAKI K, TSUNODA K, et al. ALD-Al_2O_3 passivation effects on surface characteristics of InAs/GaSb type-II superlattice infrared photodetectors[C]//Infrared Technology and Applications XLV, April 14-18, 2019, Baltimore, Maryland, USA.

[31] PLIS E, MYERS S, KHOSHAKHLAGH A, et al. InAs/GaSb strained layer superlattice detectors with nBn design[J]. Infrared physics technology, 2009, 52(6)：335-339.

[32] HOOD A, HOFFMAN D, NGUYEN B M, et al. High differential resistance type-II InAs/GaSb superlattice photodiodes for the long-wavelength infrared[J]. Applied physics letter, 2006, 89(9)：286-324.